A feasibility study of a risk-based stochastic optimization approach for radiation treatment planning under setup uncertainty

Azin Khabazian[a], Zaghian,Maryam[b], Gino J. Lim[a,*]

[a] *Department of Industrial Engineering, University of Houston, Houston, TX 77204, USA*
[b] *University of Texas MD Anderson Cancer Center, 1515 Holcombe Blvd, Houston, TX 77030, USA*

Abstract

This article introduces a planner-driven flexible stochastic decision making model to develop radiation treatment plans for cancer patients under patient-setup uncertainty. The clinical goal is to deliver the prescribed amount of radiation dose to the target tissue(s) while sparing the organs nearby. However, it is difficult to achieve the goal because organs are often closely located in the body. Therefore, some tissues may receive a higher radiation dose than desired. To minimize such violations and allow to make a trade-off between tumor coverage and healthy tissue sparing, we present a chance constrained programming (CCP) optimization method. A planner can use the CCP approach to specify how much clinical violation can be allowed for a specific patient. Assuming that the uncertain dose distribution follows a known (or estimated) probability distribution function, the CCP model was tested using five clinical cases. The resulting treatment plans were compared with the plans generated by the conventional robust worst-case optimization method using dose-volume histograms. Our results support the CCP approach over the robust optimization method in terms of healthy tissues sparing and the clinical target dose requirements. Overall, the risk-based CCP model is not only flexible to accommodate the planners risk profile and to meet patient specific treatment goals, but has potential to compromise for overly-conservative treatment plans generated by robust optimization methods.

Keywords: Chance-constrained programming, Radiation treatment planning, Risk-based approach, Setup uncertainty, Stochastic optimization.

*Corresponding author
Email addresses: azinkhabbazian@gmail.com (Azin Khabazian), MZaghian@mdanderson.org (Zaghian,Maryam), ginolim@uh.edu (Gino J. Lim)

1. Introduction

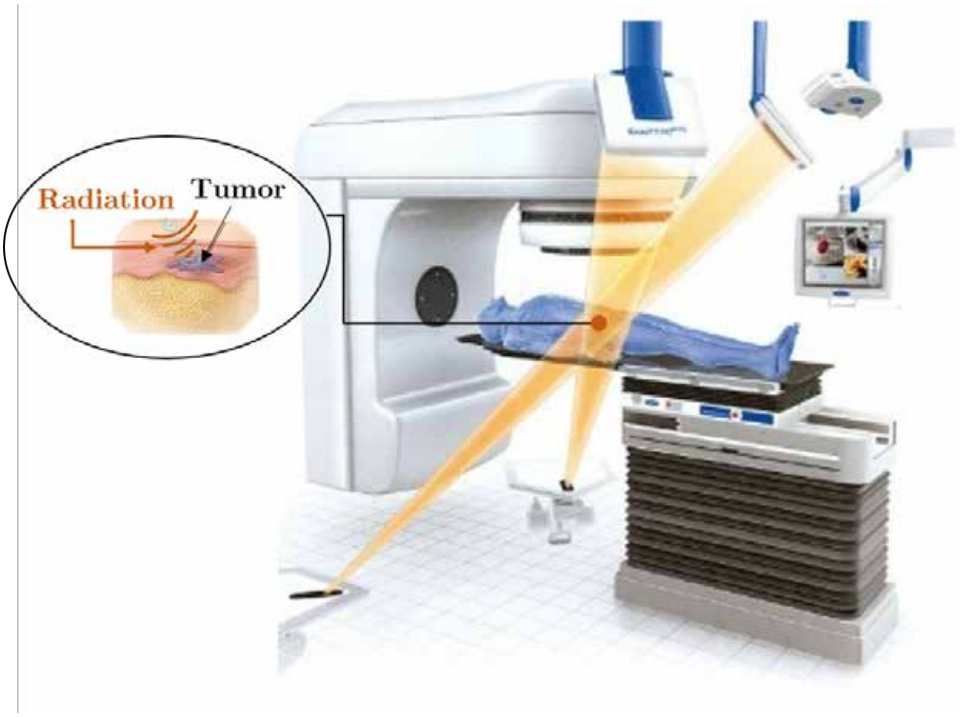

Fig. 1. Illustration of a radiation therapy treatment planning.

According to the American Cancer Society, there were around 17.0 million new cancer cases diagnosed in 2018, and radiation therapy is used in more than half of the cases, some in conjunction with chemotherapy or surgery (AmericanCancerSociety, 2018). Radiation therapy delivers radioactive particles to the tumor region to damage the DNA of the cells (see Figure 1). It is often unavoidable that the radiation can also harm healthy cells which may lead to radiation-induced side-effects (complications). The goal of radiation treatment planning is to shrink tumors (Erridge et al., 2003; Knap et al., 2010) and kill cancer cells, while minimizing negative effects on healthy organs. This can be achieved by optimally choosing the amount of radiation to be delivered to the cancerous region. Two common radiation delivery modalities are photon-based intensity modulated radiation therapy (IMRT) (Lim and Cao, 2012), and proton-based intensity-modulated proton therapy (Cao et al., 2017; Bai et al., 2018). Both methods decompose one open beam into many "beamlets" for each angle. The intensity of each beamlet can be modulated to achieve the optimal treatment effect; hence, clinical practitioners must determine how much radiation to deliver through

each beamlet (i.e., beamlet intensity or weight) so that the target volume receives the prescription dose while healthy tissues receive a minimal or no dose. This is commonly known as a fluence map optimization (FMO) problem. Over the past few years, several mathematical models have been developed for the FMO problem (Romeijn et al., 2003; Zaghian et al., 2014; Cao et al., 2017). However, in the presence of uncertainties in radiation therapy, solving the FMO problem is computationally challenging because it often involves millions of continuous and discrete variables.

Various uncertainties occur in treatment planning, such as in patient positioning, organ motion, breathing motion, dose calculation, beam energy, and others. Among these uncertainties, patient setup error is one of the most critical factors that can result in unpredictable treatment outcomes. Radiation therapy is often administered daily over a period of several weeks. For each treatment session, the patient needs to be set up on the treatment couch in the exact same position for each treatment. Due to the repeated positioning of patients, the actual and planned position of the patient with respect to the treatment can differ between each visit. As a consequence of patient setup error, the radiation dose received by each voxel can be different from the planned dose. Many existing studies highlight the importance of robustness in radiation treatment planning (Baum et al., 2006; Unkelbach and Oelfke, 2004; Bortfeld et al., 2008; Chan et al., 2006; Chu et al., 2005; Olafsson and Wright, 2006; Pflugfelder et al., 2008; Liu et al., 2012; Chan and Mišić, 2013; Fredriksson et al., 2011) and uncertainties are addressed using different models and assumptions (Shepard et al., 1999; Reemtsen and Alber, 2009).

As an extension of the deterministic (or nominal) optimization method, robust optimization (RO) is commonly used for incorporating the uncertainties in treatment planning optimization problems. An RO approach constructs a single solution that is feasible for all possible realizations of the parameter within an assumed uncertainty set. Chan et al. (2006) proposed a robust formulation of the treatment planning optimization problem using probability density functions of the uncertainty in breathing motion. Other studies have included scenario-based worst-case RO approaches (Pflugfelder et al., 2008; Liu et al., 2012; Fredriksson et al., 2011).

However, a drawback of RO is in the selection of the uncertainty set that contains all

possible realizations of the unknown parameter in the optimization model. Because it is difficult to estimate the uncertainty set, the treatment plans are often developed under the worst-case scenario (Pflugfelder et al., 2008; Chan and Mišić, 2013; Fredriksson et al., 2011). As an immediate consequence, the treatment plans can be severely conservative for the tumor region, which leads to overdose on the surrounding healthy tissues (Chen et al., 2012; Casiraghi et al., 2013; Fredriksson and Bokrantz, 2014).

In an attempt to overcome the limitations of RO and to potentially improve sparing of healthy tissues, Zaghian et al. (2018) proposed a stochastic programming approach, specifically, chance-constrained programming (CCP). A key feature of CCP is to give treatment planners control of the probability that the constraints can hold under uncertainties. Hence, with the CCP approach a user can specify a level of confidence $(1-\alpha) \in [0,1]$ for violating the constraints, where higher confidence levels result in greater avoidance of constraint violations. As a result, treatment planners can bring their own experience in to the treatment planning and have better control of tumor coverage and radiation damage to healthy tissues. A similar approach has been reported by An et al. (2017) to develop an intensity-modulated proton therapy plan using conditional-value-at-risk chance constraints. The minor drawback was that their comparison was based on the planning treatment volume-based method whereas RO is proposed to be a better approach in handling the uncertainties (Liu et al., 2012).

In CCP, an adjustable safety parameter is introduced for each of the constraints to certify the level of satisfaction on the probabilistic constraints with high confidence. These confidence levels represent prescribed safety tolerances or violation probabilities, which can provide additional information for decision makers in treatment planning. As a result, a treatment plan can be developed on the basis of the decision maker's risk preference for constraint violation while optimizing the treatment goal. In practice, the treatment goal is to spare the OARs (organs-at-risk) while delivering the prescribed dose to the tumor.

Most existing radiation treatment planning optimization models in RO do not allow constraint violation under uncertainty. But, the CCP approach allows the decision maker to adjust the level of conservatism of the robust solutions by specifying the level of constraint violations when the probability is derived with respect to sparing health organs. Therefore,

the goal of the present study is to provide flexible treatment plans in terms of OAR sparing while satisfying the clinical target dose requirements. The presented model controls the frequency of constraint violations and provides optimized treatment plans along with user-defined confidence levels with the following objectives:

- Demonstrate the effectiveness of the CCP approach in creating treatment plans that are flexible to the dose requirements of the clinician-approved trade-offs among different organs (target and OARs).
- Provide a feasibility study of the clinical implementation of the CCP approach in radiation treatment planning under uncertainty.

We performed the experiments with five clinical cases from patients who received radiation treatment for cancer to verify the impact of using the confidence-based FMO model on the optimized plan quality in terms of healthy tissue sparing.

The rest of this paper is organized as follows. In Materials and Methods, we briefly describe our FMO model in terms of the set of fixed parameters and then explain how chance constraints for treatment planning can be constructed. Under distributional assumptions of uncertainty, the deterministic equivalence of the CCP framework is also elaborated. The results for two patients with prostate cancer, one with pancreatic cancer, one pediatric patient, and one patient with lung cancer are shown and discussed in the Results. We conclude the paper with the Discussion.

2. Materials and Methods

We begin by briefly reviewing the FMO problem in radiation therapy and discussing the deterministic constraints in our optimization problem. Next, we incorporate parameter uncertainty into optimization by formulating a probabilistic version of the optimization problem. The CCP approach is then described to solve the stochastic model.

2.1. Nominal formulation

The core task of FMO in radiation treatment planning is to find the optimal value of the beamlet intensity for all beamlets. Therefore, we define decision variables representing the

intensity of beamlet $j \in \mathcal{J}$ as w_j, and the decision vector of all beamlet intensities as $\mathbf{w}$. The dose distribution is expressed as $\mathbf{D}_i(\mathbf{w})$ as a linear function of the variable w_j (Shepard et al., 1999; Lim, 2008) as follows:

$$\mathbf{D}_i(\mathbf{w}) = \sum_{j \in \mathcal{J}} d_{ij} w_j = \mathbf{d}_i^T \mathbf{w}, \ \forall i \in \{\mathcal{T} \cup \mathcal{O}\},$$

where d_{ij} denotes the dose per intensity contribution to voxel i from beamlet j. The input parameters for radiation treatment planning models proposed in the present study are defined in Table 1. A cold spot is defined as a fraction of voxels in a structure receiving less than the desired prescribed radiation dose. A hot spot is defined as a fraction of voxels in a structure receiving more than the prescribed dose.

Table 1

Input parameters for radiation treatment planning models

Symbol	Definition
$\mathcal{T}$	A set of voxels in the clinical target volume
$\mathcal{O}$	A set of voxels in an organ-at-risk
$\mathcal{J}$	A set of all beamlets
λ_T^+	Penalty coefficient for hot spots on the target
λ_T^-	Penalty coefficient for cold spots on the target
λ_O	Penalty coefficient for hot spots on an organ-at-risk
α_T^+	Risk level for having cold spots on the target
α_T^-	Risk level for having hot spots on the target
α_O^+	Risk level for having hot spots on an organ-at-risk

The deterministic FMO model in radiation therapy (Lim et al., 2008) can be represented as follows in constraints (2)-(6):

$$\min \quad -\lambda_T^- \theta_L + \lambda_T^+ \theta_U + \lambda_O^+ \varphi \tag{1}$$

s.t.

$$\mathbf{D}_i(\mathbf{w}) \geq \theta_L \qquad \forall i \in \mathcal{T} \tag{2}$$

$$\mathbf{D}_i(\mathbf{w}) \leq \theta_U \qquad \forall i \in \mathcal{T} \tag{3}$$

$$\mathbf{D}_i(\mathbf{w}) \leq \varphi, \qquad \forall i \in \mathcal{O} \tag{4}$$

$$\underline{\theta}_L \leq \theta_L \leq \bar{\theta}_L,\ \underline{\theta}_U \leq \theta_U \leq \bar{\theta}_U \tag{5}$$

$$\varphi, \mathbf{w} \geq \mathbf{0}, \tag{6}$$

in which various dose constraints are involved in the design of treatment plans. Here, θ_L (Gy) and θ_U (Gy) represent cold spot and hot spot control variables on the target, respectively, and φ (Gy) is the hot spot control variable on an organ-at-risk. Note that a cold spot is a portion of tissue that receives less than the desired radiation dose, and a hot spot is a portion of tissue that receives a dose higher than the desired dose (Lim et al., 2008). Constraint (2) ensures a high likelihood of eradicating the tumor, whereas constraint (4) ensures a high likelihood that the functionality of critical structures is retained. Constraint (3) is to avoid overdose on the target. In this optimization model, our goal is to find the beamlet intensities in such a way that deviations of the variables, θ_L, θ_U, and φ, can be minimized from their target values, i.e., $\min \theta_U - \theta_L$, $\min \varphi$. Parameters λ_T^+, λ_T^-, and λ_O^+ are for assigning different priority factors in the objective to penalize overdosing of the target, underdosing of the target, and overdosing of the OAR over the limit φ, respectively. In Constraint (5), $\underline{\theta}$ and $\bar{\theta}$ represent lower and upper bounds for variables θ_L and θ_U, respectively.

2.2. CCP formulation

Under setup uncertainty, the random dose delivered to voxel i is denoted by

$$\tilde{\mathbf{D}}_i(\mathbf{w}) = \tilde{\mathbf{d}}_i' \mathbf{w},$$

where $\tilde{\mathbf{d}}_i$ denotes the random dose contributed by all beamlets per unit weight and is received by voxel i. A classic approach to the solution of constraints (2)-(4) under random uncertainty is to enforce the constraints in probability by introducing a risk level α, which is called a chance-constrained linear program.

To construct chance constraints for radiation treatment planning optimization under patient setup uncertainty, we introduce α_i as a desired safety factor of each structure i, and

we rewrite the constraints in probability as follows:

$$P\{\tilde{\mathbf{D}}_T(\mathbf{w}) \geq \theta_L\} \geq 1 - \alpha_T^- \tag{7}$$

$$P\{\tilde{\mathbf{D}}_T(\mathbf{w}) \leq \theta_U\} \geq 1 - \alpha_T^+ \tag{8}$$

$$P\{\tilde{\mathbf{D}}_O(\mathbf{w}) \leq \varphi\} \geq 1 - \alpha_O^+. \tag{9}$$

The dose calculated using any feasible solution of constraints (7)-(9) will be between the lower and upper boundary control parameters prescribed for each structure, with a specified confidence level for each voxel. Typically, the same dose is prescribed to all voxels in the target, so we assume equal confidence levels for all voxels in the same structure for each set of constraints. In other words, the resulting dose of any feasible solution of constraints (7)-(9) is greater than θ_L with confidence level $(1-\alpha_T^-)\%$ and less than θ_U with confidence level $(1-\alpha_T^+)\%$ for the target voxel, and it is also less than φ with confidence level $(1-\alpha_O^+)\%$ for each OAR voxel, in the face of uncertainty.

Unfortunately, there is often a conflict between the lower and upper bound constraints, which will lead to an infeasible solution in practice. To avoid infeasibility of the optimization problem, we may allow some or all of these constraints to be violated up to a certain level. We can easily penalize the violations of the lower and upper bounds on the amount of dose received by each voxel in the objective function. In this regard, assuming that confidence levels $(1-\alpha_i)$ are given, we developed model (10), in which θ_L, θ_U, and φ are considered as decision variables.

$$\begin{aligned}
&\min \quad -\lambda_T^-\,\theta_L + \lambda_T^+\,\theta_U + \lambda_O^+\,\varphi && && (10)\\
&s.t. && &&\\
&P\{\tilde{\mathbf{D}}_T(\mathbf{w}) \geq \theta_L\} \geq 1-\alpha_T^-, && \forall i \in \mathcal{T} &\\
&P\{\tilde{\mathbf{D}}_T(\mathbf{w}) \leq \theta_U\} \geq 1-\alpha_T^+, && \forall i \in \mathcal{T} &\\
&P\{\tilde{\mathbf{D}}_O(\mathbf{w}) \leq \varphi\} \geq 1-\alpha_O^+, && \forall i \in \mathcal{OAR} &\\
&Constraints\ (5)-(6), && &
\end{aligned}$$

Next, we solve the CCP model (10) by treating uncertain parameters as continuous random variables with a known probability density function.

2.3. CCP models under distributional assumptions

One of the computational challenges in solving a CCP model comes from the fact that the chance constraints may not be convex (Nemirovski and Shapiro, 2006). However, a CCP model can be made convex in a few special cases. For example, if the uncertainty parameter ($\tilde{\mathbf{d}}_i$) has a log-concave probability density, the corresponding chance constraints will be convex (Zaghian et al., 2018).

In this section, we consider two special probability distribution functions of random parameter $\tilde{\mathbf{d}}_i$, normal and uniform distribution. We focus on the normal distribution because it is widely used and has attractive analytical properties that facilitate further analysis (Chan et al., 2009). As follows from the central limit theorem (Bertsekas and Tsitsiklis, 2002), a large set of independent identically distributed random variables approach a normal distribution regardless of the underlying probability distribution. So, the normality assumption will also help extend the analysis to multiple sources of uncertainty. Thus, we constructed the deterministic equivalent of a CCP framework on the basis of the normality assumption of a random parameter (Zaghian et al., 2018) (see Appendix A) as well as a uniform distribution (see Appendix B). Note that we used normal and uniform probability distributions that are widely used in practice as an example to describe the setup uncertainty (Chan et al., 2009; Engelsman et al., 2005).

3. Clinical cases and planning details

We evaluated the relative performance of the CCP models on the basis of treatment plan information obtained from five cancer patients (two patients with prostate cancer, one with pancreatic cancer, one pediatric patient, and one patient with lung cancer) who received radiation therapy at The University of Texas MD Anderson Cancer Center.

By assuming that the setup uncertainty ranged between -5 mm and $+5$ mm (Manning et al., 2001; Wong et al., 2005), we generated four representative scenarios in addition to the nominal scenario (Liu et al., 2012; Casiraghi et al., 2013) for the patient setup uncertainty. The first- and second-order moments of the uncertain dose contributions were calculated for each case under normal and uniform distributional assumptions. Under these assumptions, the respective minimum and maximum doses to the target were 95% ($\underline{\theta}_L = 0.95$) and 105%

($\bar{\theta}_U = 1.05$) of the prescribed dose in all plans. The values of weight factors λ_T^-, λ_T^+, and λ_O^+ are often selected on the basis of the planner's preference. Table 2 lists the planning parameters for the five clinical cases analyzed in the present study. For each case, the number of beams, number of voxels within each volume, and the corresponding dose-volume requirements were provided.

Table 2

Anatomical structures and dose requirements for five clinical cases used in our analysis

Cancer Case [1]	Volume	NO. of Beams	Constraints
Prostate I (IMRT)	Target: 1000	6	Prescription: 76 Gy
			Receiving $\geq$ 96% of θ_L
			Receiving $\leq$ 105% of θ_U
	OAR (rectum): 5848		
	OAR (bladder): 10603		
Prostate II (IMRT)	Target: 6375	6	Prescription: 76 Gy
			Receiving $\geq$ 95% of θ_L
			Receiving $\leq$ 105% of θ_U
	OAR (rectum): 5719		
	OAR (bladder): 7850		
Pancreas (IMRT)	Target: 1244	12	Prescription: 54 Gy
			Receiving $\geq$ 99% of θ_L
			Receiving $\leq$ 101% of θ_U
	OAR (liver): 50391		
	OAR (spinal cord): 489		Max dose: 45 Gy
	OAR (left kidney): 9116		
	OAR (right kidney): 5920		
Lung (IMPT)	Target: 5716	3	Prescription: 70 Gy
			Receiving $\geq$ 95% of θ_L
			Receiving $\leq$ 107% of θ_U
	OAR (heart): 8287		
	OAR (spinal cord): 481		
	OAR (esophagus): 389		
Pediatric (IMPT)	Target: 9307	3	Prescription: 64 Gy
			Receiving $\geq$ 95% of θ_L
			Receiving $\leq$ 105% of θ_U
	OAR (brainstem): 1118		
	OAR (optic chiasm): 17		

Different treatment plans were generated for each of the clinical cases: one with the deterministic approach, one with the robust worst-case optimization and the others using the CCP treatment planning models. The models were solved using a commercial linear optimization solver, CPLEX (IBM Analytics, Accessed April 11, 2018). Note that the beam angles were optimized (Lim et al., 2014) and confirmed by clinicians in advance.

A family of dose-volume histograms (DVHs) for the comparison of different models were applied. We used the DVH family band width method (Trofimov et al., 2012) that displayed all DVHs of the five dose distributions corresponding to the four scenarios of setup uncertainty in addition to the nominal scenario. DVH indices comparing tumor dose coverage, homogeneity, and OAR sparing are also discussed in detail in the next section.

4. Results

4.1. Plan quality and robustness

Plans optimized by the chance-constrained and nominal (or deterministic) optimization models for one of the patients with prostate cancer are compared in Figures 2a-2f. The DVHs corresponding to the nominal dose distribution (i.e., no uncertainty) are displayed along with the DVH bands for deterministic and chance-constrained models. The solid line indicates DVHs for the nominal dose distribution and the shaded area shows the DVH family band plotted on the basis of various shifted setup scenarios. For all plans, the nominal DVHs (solid lines) were almost equally good, which shows that the clinical constraints were satisfied. However, Figure 2a shows that the band of the DVH along the target is wider for the deterministic model than for the CCP models (DVHs in Figures 2c and 2e), which shows that the target coverage of the deterministic model was worse than that of the CCP models.

Moreover, as would be expected, the DVH bands on OARs that are illustrated on the right side of Figure 2 are reduced by the CCP approach under two different distributional assumptions. In fact, these figures explain how controlling the violation of the clinical constraints using CCP models resulted in improved OAR sparing compared with the deterministic model. Overall, this comparison demonstrates that by incorporating setup uncertainty information in the optimization, the sensitivity of the plans against errors can be reduced.

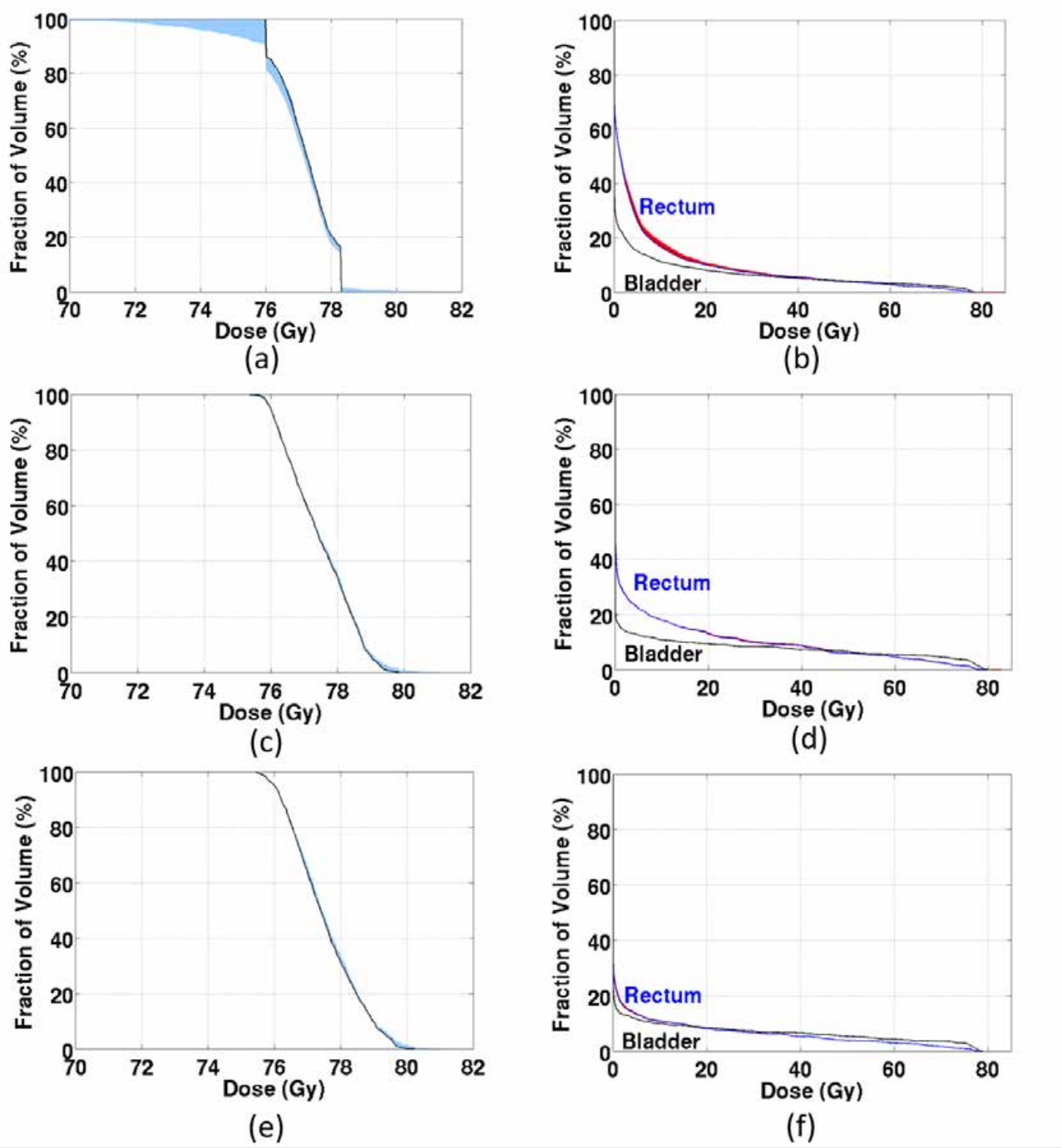

Fig. 2. Dose-volume histogram bands for target and organs-at-risk dose distributions covering all setup uncertainties, resulting from (a, b) the deterministic approach, (c, d) chance-constrained programming under the normality assumption, and (e, f) chance-constrained programming under the uniformity assumption. The straight vertical line at dose 76 Gy and around 78 Gy is the direct result of using a linear programming (LP)-based model that imposes a linear penalty on all deviations and focuses more on minimizing the upper limit and maximizing the lower limit for the target (Zaghian et al., 2017).

4.2. Robust optimization:

The plans were optimized to evaluate the robustness of treatment plans using CCP and RO under random setup errors, and corresponding DVHs for the target and OARs were analyzed for each of the setup scenarios.

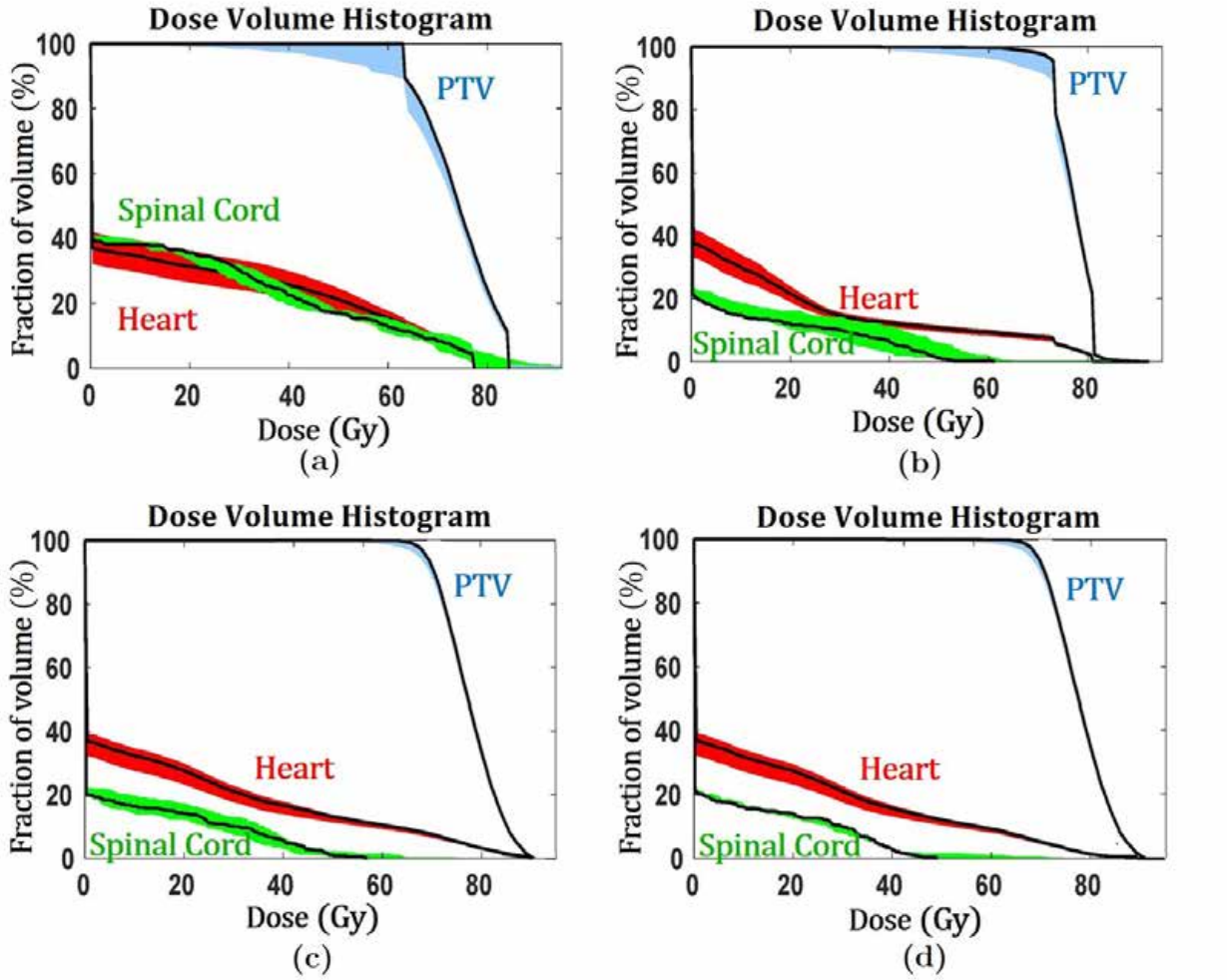

Fig. 3. Lung cancer dose-volume histogram bands for planned target volume (PTV) and organs-at-risk dose distributions covering all setup uncertainties, resulting from (a) the deterministic approach, (b) robust optimization, (c) chance-constrained programming under the normality assumption, and (d) chance-constrained programming under the uniformity assumption.

Figure 3 shows the DVH family band for the lung cancer case, based on treatment plans developed using the deterministic approach, RO, and CCP under normal (CCP-N) and CCP under uniform probability distributions (CCP-U). Figures in Appendix C show the results for the two prostate cancer cases, the pancreatic, and the pediatric cancer cases, respectively.

The DVHs in Figure 3 show that all nominal plans (black line) met the clinical prescription criteria in both covering the tumor and sparing OARs, and the target was robustly covered for all plans, as indicated by the narrow DVH family band (shaded area) compared with the deterministic approach. Based on the experiments presented in the paper, the confidence-based CCP models outperformed the robustly optimized plan by improving the protection of critical organs under the nominal and setup scenarios. The shaded area around the nominal DVHs of the spinal cord in the robust plan (Figure 3b) is wider than that in the CCP plans (Figure 3c and 3d). As shown in Figures 3c and 3d, the maximum doses to the normal cells around the target from the CCP plans met the tolerances without sacrificing the robustness of the plan to setup uncertainty, which demonstrates the flexibility of the CCP approach compared to the RO method in creating clinically reasonable plans.

To further illustrate the performance of the biologically-based CCP models, we explored the effect of CCP models on sparing of normal tissues around the tumor for the five clinical cases. Table 3 reports radiation dose statistics associated with OAR DVHs for each case based on the plans optimized by the CCP models and worst-case RO approach. The values in the nominal scenario as well as the average and worst-case values considering all setup scenarios are presented. The table shows that the proposed CCP models delivered smaller radiation doses to the normal organs than the RO approach for all cases for each of the three measures: nominal, worst-case, and average dose.

Table 3 shows the radiation dose statistics on healthy organs for all cancer cases as explained by An et al. (2017): D_1 (Gy), the amount of dose received by more than 1% of the organ. The CCP approach reduced the nominal dose of D_1 for the rectum in Prostate case I as compared to RO: 75.64 Gy for CCP-N and 72.39 Gy (vs. 76.46) in case of CCP-U. The average dose of D_1 (Gy) on the bladder was also reduced when the CCP approach was used on each of the nominal, worst-case, and average scenario. We observed similar results for Prostate case II shown in Table 3. For the Pancreas case, the maximum nominal doses of D_1 on healthy organs were 35.42 Gy and 28.46 Gy for liver and spinal cord using the RO model, respectively. Those values were reduced to 22.48 Gy and 28.05 Gy using CCP-N, and to 23.51 Gy and 28.10 Gy using the CCP-U model for the liver and spinal cord, respectively. Similar results were observed by comparing the results of maximum dose (D_1 (Gy)) on the

liver and spinal cord for worst-case and average case scenarios. For this case, the maximum radiation dose on the spinal cord was slightly lower for CCP plans, whereas there were significant improvements in protecting the liver by reducing the amount by at least 12.94 Gy when compared to the RO plan. For a better illustration of the dose volume histogram plotted for the liver in the Pancreas case, the percentage of the liver volume receiving more than 30 Gy, $V_{30}\%$, was compared for all the plans. Both CCP-N and CCP-U reduced $V_{30}\%$ by 2.18% and 2.03%, respectively, over the robust plan. It can be seen that the CCP plans delivered the least amount of dose to the healthy tissue, especially, in the liver. For the case of the lung cancer, the CCP result in a slightly higher dose of D_1 (Gy) (maximum dose) for the heart. However, this was a necessary compromise to provide a plan with better sparing of the spinal cord, which can be severely damaged if it is over-dosed.

Both CCP under the normality assumption and CCP under the uniformity assumption appeared to provide better control than the RO approach in terms of sparing of normal tissues, which can be achieved by controlling the tolerance levels assigned to each structure's dose requirements and studying the relationship between dose requirements and plan conservatism. In a CCP setting, the confidence level of satisfying the target dose requirement can be adjusted on the basis of the physician's preference to avoid overly conservative treatment plans. As a result, with the CCP method the OAR protection can be improved, and this will prevent side effects due to radiation and lead to better quality of life for patients.

Table 3

Comparison of chance-constrained models (CCP-N and CCP-U with $\alpha = 95\%$) and the worst-case robust optimization (RO) method on healthy organ sparing. The values are derived from the dose-volume histograms.[2]

	Prostate I		**Prostate II**		**Pancreas**		
	Rectum	**Bladder**	**Rectum**	**Bladder**	**Liver**		**Spinal Cord**
CCP-N	D_1 (Gy)	D_1 (Gy)	D_1 (Gy)	D_1 (Gy)	$V_{30}\%$	D_1 (Gy)	D_1 (Gy)
nominal	75.64	77.27	77.35	77.19	0.23	22.48	28.05
worst-case	75.93	77.27	77.36	77.31	0.35	23.20	28.24
average	75.74	77.22	77.33	77.22	0.26	22.76	28.12
CCP-U							
nominal	72.39	77.25	76.97	77.69	0.38	23.51	28.10
worst-case	72.88	77.29	77.06	77.72	0.46	24.34	29.33
average	72.51	77.24	76.98	77.69	0.39	23.71	28.36
RO							
nominal	76.46	77.27	77.39	78.24	2.41	35.42	28.46
worst-case	77.45	77.38	77.76	78.24	2.73	36.60	32.00
average	76.71	77.28	77.46	78.24	2.50	35.88	29.84

	Lung			**Pediatric**	
	Heart	**Spinal Cord**		**Brainstem**	**Optic Chiasm**
CCP-N	D_1 (Gy)	D_1 (Gy)	$V_{40}\%$	D_1 (Gy)	D_1 (Gy)
nominal	85.03	49.88	5.40	60.92	14.38
worst-case	85.03	61.88	6.44	61.24	14.68
average	84.50	51.18	5.02	61.07	14.44
CCP-U					
nominal	81.23	44.52	2.70	60.92	14.38
worst-case	82.22	59.52	2.91	61.24	14.64
average	81.23	47.63	2.74	60.91	14.44
RO					
nominal	81.05	50.21	6.02	61.24	14.38
worst-case	81.15	61.79	11.23	61.24	14.70
average	81.10	53.26	6.44	61.23	14.50

Next, we evaluated the robustness of the CCP plans in terms of tumor dose coverage. Table 4 shows the tumor DVH indices achieved by our confidence-based CCP models and

[2] D_1 denotes the amount of dose received by more than 1% percent of the organ, and $V_{30}\%$ denotes the percentage of the organ volume receiving dose of more than 30 Gy.

worst-case RO approach. For each clinical case, the first row shows the dose homogeneity index (HI) that is often used as an objective measure of treatment plan quality (Yoon et al., 2007). HI is calculated by

$$HI = \frac{D_{95}}{D_5},\ 0 \leq HI \leq 1,$$

where D_5 and D_{95} are the dose coverage at 5% and 95% volume of the target: the larger (closer to 1) the value of HI, the better the dose homogeneity.

To quantify the plan robustness under uncertainty, we listed the width of the DVH band at D_5 and D_{95} in the second and third rows. The nominal HI values for all clinical cases except the patient with lung cancer were equally high, and the DVH band-widths from the CCP models were better than those from the RO model (as shown in Figure 3 and figures in Appendix C). For the patient with lung cancer, the nominal HI values were slightly lower for the CCP plans, whereas the indices of DVH band width from the CCP models outperformed those from the RO plan. This means that the target coverage of the plans generated by the CCP models under two different distributional assumptions was more robust when compared with the RO plan for shifted setup uncertainty.

Table 4

Homogeneity index for clinical cases examined in our analysis.

Case[3]		CCP-N	CCP-U	RO
Prostate cancer I	HI (nominal)	0.96	0.95	0.96
	D_5 DVH band	0.05	0.05	0.05
	D_{95} DVH band	0.01	0.05	0.01
Prostate cancer II	HI (nominal)	0.96	0.96	0.96
	D_5 DVH band	0.03	0.05	0.05
	D_{95} DVH band	0.01	0.02	0.02
Pancreatic cancer	HI (nominal)	0.97	0.97	0.97
	D_5 DVH band	0.10	0.15	0.26
	D_{95} DVH band	0.15	0.20	0.35
Lung cancer	HI (nominal)	0.88	0.88	0.90
	D_5 DVH band	0.15	0.13	0.15
	D_{95} DVH band	3.00	3.54	9.19
Pediatric cancer	HI (nominal)	0.86	0.86	0.86
	D_5 DVH band	0.12	0.15	0.16
	D_{95} DVH band	0.05	0.03	0.04

4.3. Sensitivity Analysis

This section discusses the sensitivity of CCP models to the choice of a distribution. We designed an experiment to test the performance of the proposed model when the assumed dose distribution for treatment planning was different from the true distribution, which is not known in advance. For example, treatment plans may have been developed based on the assumption that the set up error follows a normal distribution (CCP-N) when, in fact, the true probability distribution was Uniform. The parameter values resulting from those experiments on Prostate case I are shown in Table 5.

[3]HI:homogeneity index, DVH: dose-volume histogram

Table 5

Cold- and hot-spot control parameters on target (θ_L and θ_U) and hot-spot control parameter on OARs (φ) optimized for Prostate I.

Assumption	Approach	θ_L (Gy)	θ_U (Gy)	φ (Gy)
Normally distributed	CCP-N	76.00	77.52	76.00
	CCP-U	72.20	81.32	79.04
Uniformly distributed	CCP-N	76.00	82.08	78.28
	CCP-U	74.48	76.00	74.48

First, we compare the treatment plans under the two distributional assumptions in terms of the *uniformity* of the planned dose distribution on the target (Lim et al., 2007). In radiation therapy, the uniformity is the difference between the maximum dose and the minimum dose received on the target, which is measured by $\theta_U - \theta_L$. Ideally, we wish to achieve a treatment plan whose gap is close to zero. In Table 5, when the random data was assumed to follow a normal probability distribution, the uniformity value of the CCP-N based treatment plan (i.e., $1.52\ Gy = 77.52 - 76.00$) is smaller than the CCP-U based plan ($9.12\ Gy = 81.32 - 72.20$). However, when the random data was assumed to follow a uniform probability distribution, we observed the opposite result as the uniformity value of CCP-N (6.08) is larger than that of CCP-U (1.52).

Next, we compared the performance of the proposed model (CCP-N/CCP-U) with the maximum threshold on OARs obtained based on the respective distributional assumption. As it is shown from the last column of Table 5, the plan by CCP-N resulted in a consistently lower upper threshold limit on OARs ($\varphi = 76.00$ Gy) than did CCP-U ($\varphi = 79.04$ Gy) under the normal probability distribution assumption. A similar observation was made when the random parameter was assumed to follow a uniform distribution (from the last two rows in Table 5).

5. Discussion

In the present work, we explored the CCP optimization framework using five clinical cases. Treatment plans were optimized for robustness, quality, and homogeneity under patient setup

errors. In practice, the treatment goal is to spare the OARs while delivering the prescribed dose to the tumor. However, these conflicting objectives are often difficult to achieve. In a worst-case scenario, critical organs will necessarily receive more doses when a plan robustly covers the target. Conversely, the target will not receive a sufficient radiation dose when a plan robustly spares a nearby critical structure. Thus, the level of the plan conservatism needs to be determined under uncertainty, and this can be decided by adjusting the tolerance levels introduced in the CCP approach. Our results showed that the confidence-based CCP model was a user-centric optimization tool that can help obtain a good balance between the plan quality and robustness. Our analysis covered five clinical cases under two probability assumptions of random setup uncertainty using the same clinical limitations and directions. Our numerical results for the clinical cases showed that the CCP approach was capable of controlling the robustness of the model while attaining high-quality solutions. We believe that the CCP plans demonstrated here will be applicable to many different types of clinical cases under different probability assumptions of uncertainty.

Appendix A

CCP model under Normal distribution (CCP-N)

First, consider dose contribution vector $\tilde{\mathbf{d}}_i$ is assumed to be normally distributed with mean $E(\tilde{\mathbf{d}}_i)$ and standard deviation $\sigma(\tilde{\mathbf{d}}_i)$. So, we have

$$
\begin{aligned}
&\min \quad -\lambda_T^- \,\theta_L + \lambda_T^+ \,\theta_U + \lambda_O^+ \,\varphi && && (11)\\
&s.t. \\
&E(\tilde{\mathbf{D}}_T(\mathbf{w})) - \Phi^{-1}(1-\alpha_T^-)\sigma(\tilde{\mathbf{D}}_T(\mathbf{w})) \geq \theta_L && \forall\, \mathcal{T} \\
&E(\tilde{\mathbf{D}}_T(\mathbf{w})) + \Phi^{-1}(1-\alpha_T^+)\sigma(\tilde{\mathbf{D}}_T(\mathbf{w})) \leq \theta_U && \forall\, \mathcal{T} \\
&E(\tilde{\mathbf{D}}_O(\mathbf{w})) + \Phi^{-1}(1-\alpha_O^+)\sigma(\tilde{\mathbf{D}}_O(\mathbf{w})) \leq \varphi && \forall\, \mathcal{O} \\
&\underline{\theta}_L \leq \theta_L \leq \bar{\theta}_L,\ \underline{\theta}_U \leq \theta_U \leq \bar{\theta}_U \\
&\varphi, \mathbf{w} \geq 0
\end{aligned}
$$

as a deterministic equivalent of CCP model (10). The cumulative distribution of a normal standard probability density is represented with $\Phi(\cdot)$.

Appendix B

CCP model under uniform distribution (CCP-U)

Similarly, under uniform distributional assumption, the deterministic linear equivalents of the chance constraints (10) are provided.

Assuming, vector $\tilde{\mathbf{d}}_i - E(\tilde{\mathbf{d}}_i)$ is distributed uniformly in the ellipsoid $\varepsilon = \{\xi = Qz : \|z\| \leq 1\}$, where $Q = \upsilon\Gamma_f, \Gamma = \sigma^2(\tilde{d}_i) \succ 0, \upsilon = \sqrt{n+3}, \Gamma_f \in R^n$, and υ is a full rank factor such that $\Gamma = \Gamma_f\Gamma_f^T$, the deterministic equivalence of model (10) can be formulated as follows:

$$
\begin{aligned}
\min \quad & -\lambda_T^- \theta_L + \lambda_T^+ \theta_U + \lambda_O^+ \varphi && (12)\\
s.t. & \\
& E(\tilde{\mathbf{D}}_T(\mathbf{w})) - \upsilon\sqrt{\Psi_{beta}^{-1}(1-2\alpha_T^-)}\,\sigma(\tilde{\mathbf{D}}_T(\mathbf{w})) \geq \theta_L \qquad \forall\mathcal{T}\\
& E(\tilde{\mathbf{D}}_T(\mathbf{w})) + \upsilon\sqrt{\Psi_{beta}^{-1}(1-2\alpha_T^+)}\,\sigma(\tilde{\mathbf{D}}_T(\mathbf{w})) \leq \theta_U \qquad \forall\mathcal{T}\\
& E(\tilde{\mathbf{D}}_O(\mathbf{w})) + \upsilon\sqrt{\Psi_{beta}^{-1}(1-2\alpha_O^+)}\,\sigma(\tilde{\mathbf{D}}_O(\mathbf{w})) \leq \varphi \qquad \forall\mathcal{O}\\
& \underline{\theta}_L \leq \theta_L \leq \bar{\theta}_L,\ \underline{\theta}_U \leq \theta_U \leq \bar{\theta}_U\\
& \varphi, \mathbf{w} \geq 0
\end{aligned}
$$

where $\Psi_{beta}(\cdot)$ is the cumulative distribution of a $\beta(1/2; n/2+1)$ probability density.

Models (11) and (12) were developed to optimize the thresholds (θ_L, θ_U, and φ) of the constraints while guaranteeing the constraints hold a pre-specified probability.

Appendix C

Dose-volume histogram for the prostate cancer cases, the pancreatic, and pediatric cancer cases

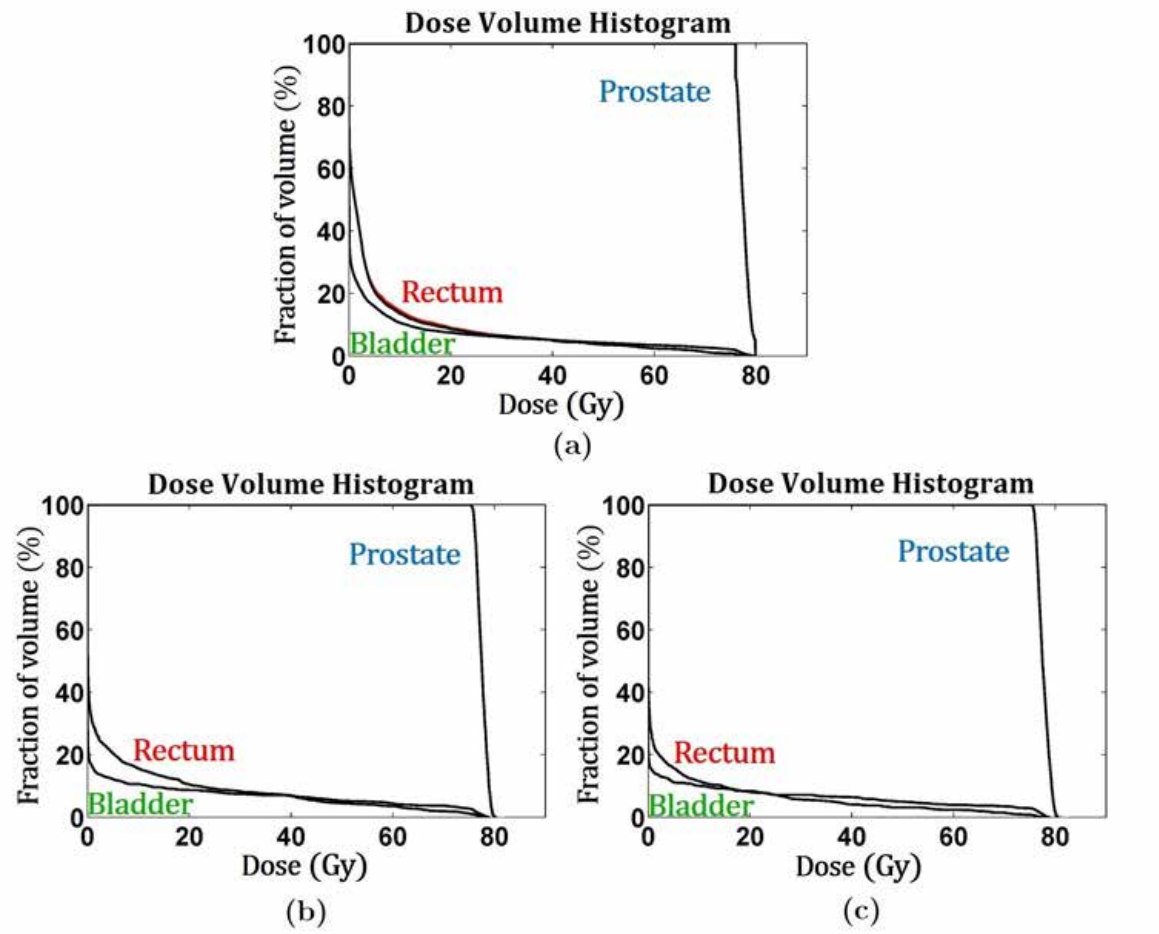

Fig. C. Prostate cancer (case I) dose-volume histogram bands for target and organs-at-risk dose distributions covering all setup uncertainties, resulting from (a) robust optimization, (b) chance-constrained programming under the normality assumption, and (c) chance-constrained programming under the uniformity assumption.

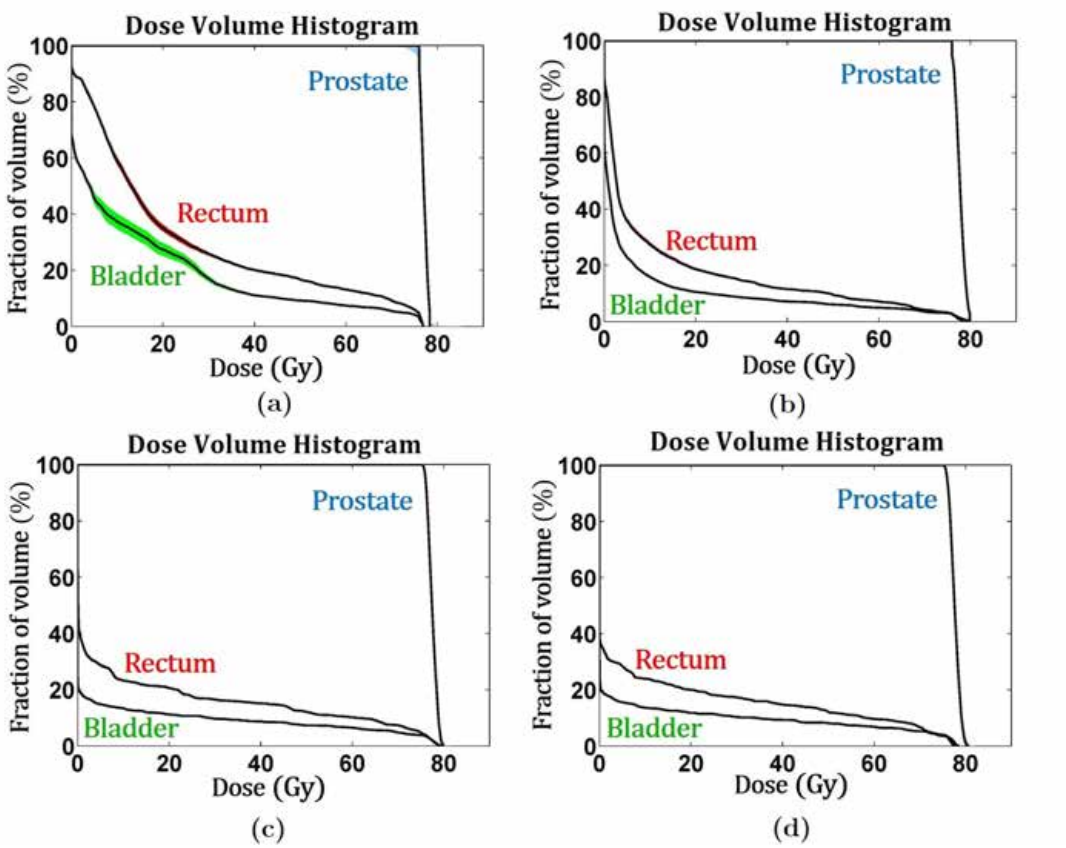

Fig. C. Prostate cancer (case II) dose-volume histogram bands for target and organs-at-risk dose distributions covering all setup uncertainties, resulting from (a) the deterministic approach, (b) robust optimization, (c) chance-constrained programming under the normality assumption, and (d) chance-constrained programming under the uniformity assumption.

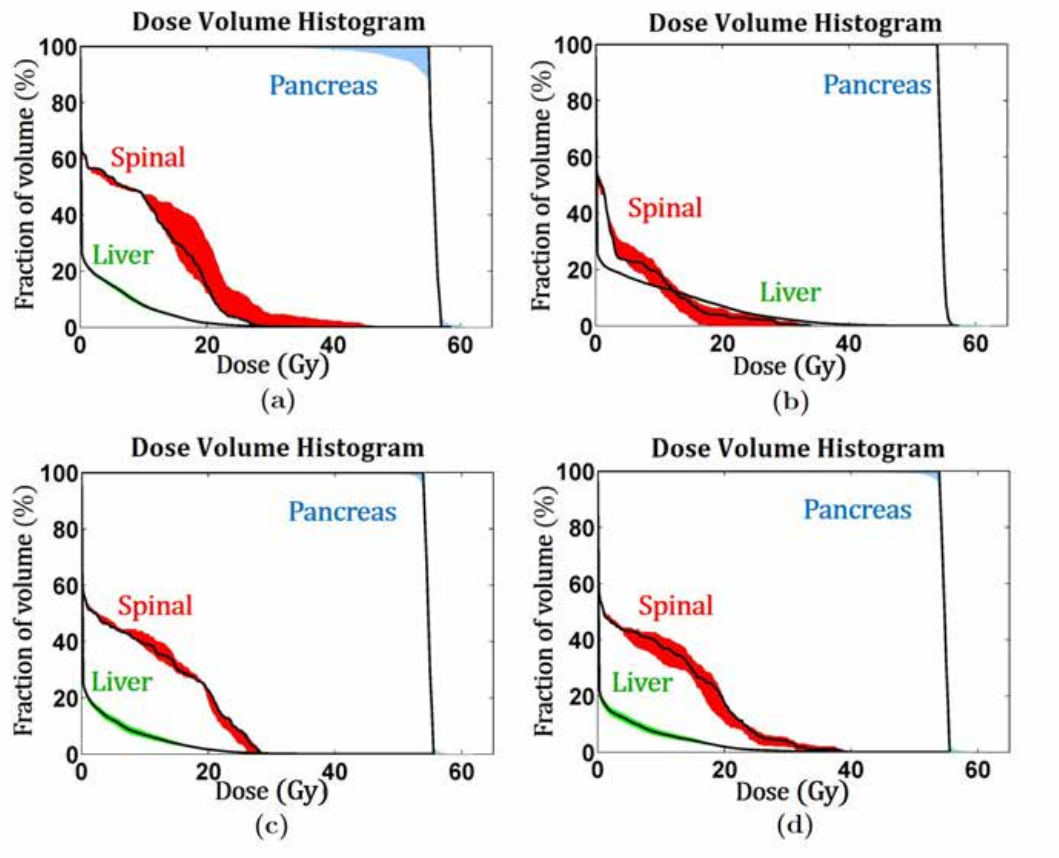

Fig. C. Pancreatic cancer dose-volume histogram bands for target and organs-at-risk dose distributions covering all setup uncertainties, resulting from (a) the deterministic approach, (b) robust optimization, (c) chance-constrained programming under the normality assumption, and (d) chance-constrained programming under the uniformity assumption.

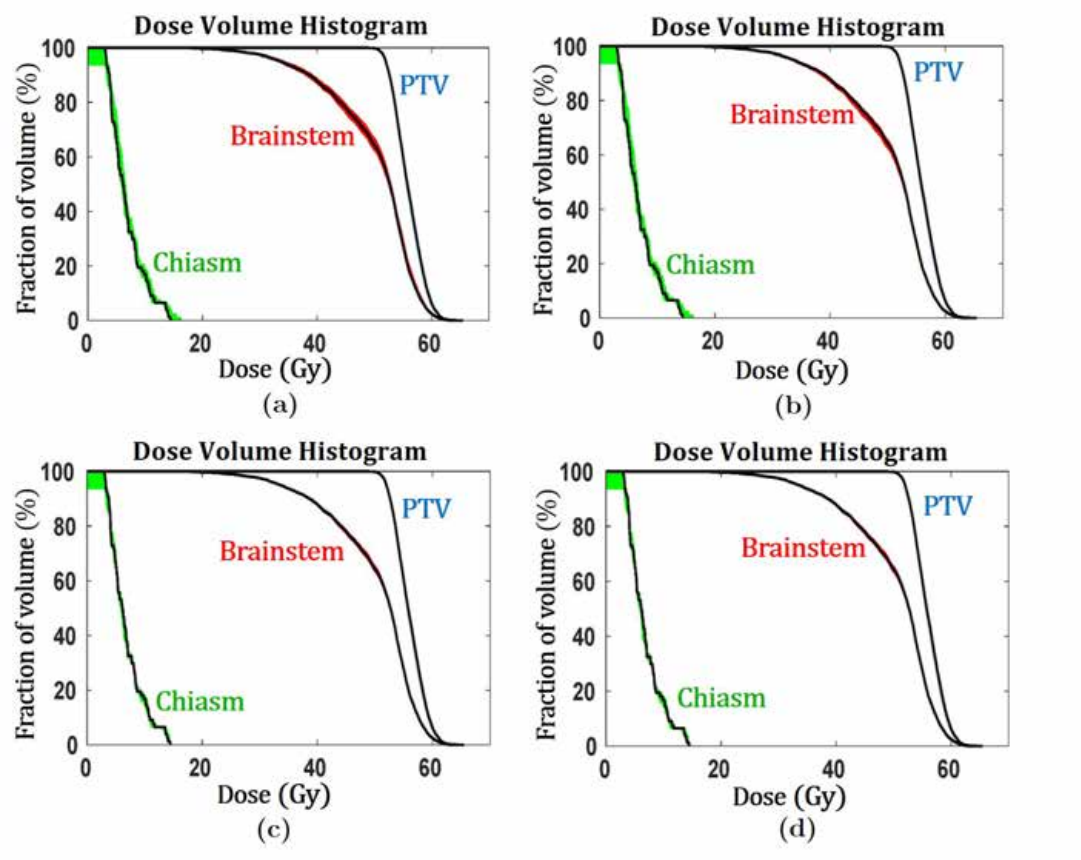

Fig. C. Pediatric cancer dose-volume histogram bands for target and organs-at-risk dose dose distributions covering all setup uncertainties, resulting from (a) the deterministic approach, (b) robust optimization, (c) chance-constrained programming under the normality assumption, and (d) chance-constrained programming under the uniformity assumption.

AmericanCancerSociety, 2018. Cancer facts and figures. www.cancer.orgresearchcancerfactsfiguresacspc-031941.

An, Y., Liang, J., Schild, S. E., Bues, M., Liu, W., 2017. Robust treatment planning with conditional value at risk chance constraints in intensity-modulated proton therapy. Medical Physics 44 (1), 28–36.

Bai, X., Lim, G. J., Grosshans, D. R., Mohan, R., Cao, W., 2018. Robust optimization to reduce the impact of biological effect variation from physical uncertainties in intensity-modulated proton therapy. Physics in medicine and biology.

Baum, C., Alber, M., Birkner, M., Nüsslin, F., 2006. Robust treatment planning for intensity modulated radiotherapy of prostate cancer based on coverage probabilities. Radiotherapy and Oncology 78 (1), 27–35.

Bertsekas, D. P., Tsitsiklis, J. N., 2002. Introduction to probability. Vol. 1. Athena Scientific Belmont, MA.

Bortfeld, T., Chan, T. C., Trofimov, A., Tsitsiklis, J. N., 2008. Robust management of motion uncertainty in intensity-modulated radiation therapy. Operations Research 56 (6), 1461–1473.

Cao, W., Khabazian, A., Yepes, P. P., Lim, G., Poenisch, F., Grosshans, D. R., Mohan, R., 2017. Linear energy transfer incorporated intensity modulated proton therapy optimization. Physics in Medicine and Biology 63 (1), 015–013.

Casiraghi, M., Albertini, F., Lomax, A., 2013. Advantages and limitations of the worst case scenario approach in IMPT treatment planning. Physics in Medicine & Biology 58 (5), 1323.

Chan, T. C., Bortfeld, T., Tsitsiklis, J. N., 2006. A robust approach to IMRT optimization. Physics in Medicine and Biology 51 (10), 2567.

Chan, T. C., Mišić, V. V., 2013. Adaptive and robust radiation therapy optimization for lung cancer. European Journal of Operational Research 231 (3), 745–756.

Chan, T. C., Tsitsiklis, J. N., Bortfeld, T., 2009. Optimal margin and edge-enhanced intensity maps in the presence of motion and uncertainty. Physics in Medicine and Biology 55 (2), 515.

Chen, W., Unkelbach, J., Trofimov, A., Madden, T., Kooy, H., Bortfeld, T., Craft, D., 2012. Including robustness in multi-criteria optimization for intensity-modulated proton therapy. Physics in Medicine & Biology 57 (3), 591.

Chu, M., Zinchenko, Y., Henderson, S. G., Sharpe, M. B., 2005. Robust optimization for intensity modulated radiation therapy treatment planning under uncertainty. Physics in Medicine and Biology 50 (23), 5463.

Engelsman, M., Sharp, G., Bortfeld, T., Onimaru, R., Shirato, H., 2005. How much margin reduction is possible through gating or breath hold? Physics in Medicine and Biology 50 (3), 477.

Erridge, S. C., Seppenwoolde, Y., Muller, S. H., van Herk, M., De Jaeger, K., Belderbos, J. S., Boersma, L. J., Lebesque, J. V., 2003. Portal imaging to assess set-up errors, tumor motion and tumor shrinkage during conformal radiotherapy of non-small cell lung cancer. Radiotherapy and Oncology 66 (1), 75–85.

Fredriksson, A., Bokrantz, R., 2014. A critical evaluation of worst case optimization methods for robust intensity-modulated proton therapy planning. Medical physics 41 (8Part1), 081701.

Fredriksson, A., Forsgren, A., Hårdemark, B., 2011. Minimax optimization for handling range and setup uncertainties in proton therapy. Medical Physics 38 (3), 1672–1684.

IBM Analytics, Accessed April 11, 2018. The ilog cplex. www.ilog.com/products/cplex/.

Knap, M. M., Hoffmann, L., Nordsmark, M., Vestergaard, A., 2010. Daily cone-beam computed tomography used to determine tumour shrinkage and localisation in lung cancer patients. Acta Oncologica 49 (7), 1077–1084.

Lim, G., 2008. An Introduction to Radiation Therapy Planning Optimization. Optimization in Medicine and Biology 16, 197–221.

Lim, G. J., Cao, W., 2012. A two-phase method for selecting imrt treatment beam angles: Branch-and-prune and local neighborhood search. European Journal of Operational Research 217 (3), 609–618.

Lim, G. J., Choi, J., Mohan, R., 2008. Iterative solution methods for beam angle and fluence map optimization in intensity modulated radiation therapy planning. OR Spectrum 30 (2), 289–309.

Lim, G. J., Ferris, M. C., Shepard, D. M., Wright, S. J., Earl, M. A., 2007. An optimization framework for conformal radiation treatment planning. INFORMS Journal on Computing 19 (3), 366–380.

Lim, G. J., Kardar, L., Cao, W., 2014. A hybrid framework for optimizing beam angles in radiation therapy planning. Annals of Operations Research 217 (1), 357–383.

Liu, W., Zhang, X., Li, Y., Mohan, R., 2012. Robust optimization of intensity modulated proton therapy. Medical physics 39 (2), 1079–1091.

Manning, M. A., Wu, Q., Cardinale, R. M., Mohan, R., Lauve, A. D., Kavanagh, B. D., Morris, M. M., Schmidt-Ullrich, R. K., 2001. The effect of setup uncertainty on normal tissue sparing with IMRT for head-and-neck cancer. International Journal of Radiation Oncology* Biology* Physics 51 (5), 1400–1409.

Nemirovski, A., Shapiro, A., 2006. Convex approximations of chance constrained programs. SIAM Journal on Optimization 17 (4), 969–996.

Olafsson, A., Wright, S. J., 2006. Efficient schemes for robust IMRT treatment planning. Physics in Medicine and Biology 51 (21), 5621.

Pflugfelder, D., Wilkens, J., Oelfke, U., 2008. Worst case optimization: a method to account for uncertainties in the optimization of intensity modulated proton therapy. Physics in Medicine and Biology 53 (6), 1689.

Reemtsen, R., Alber, M., 2009. Continuous optimization of beamlet intensities for intensity modulated photon and proton radiotherapy. In: Handbook of Optimization in Medicine. Springer, pp. 1–40.

Romeijn, H. E., Ahuja, R. K., Dempsey, J. F., Kumar, A., Li, J. G., 2003. A novel linear programming approach to fluence map optimization for intensity modulated radiation therapy treatment planning. Physics in Medicine and Biology 48 (21), 3521.

Shepard, D. M., Ferris, M. C., Olivera, G. H., Mackie, T. R., 1999. Optimizing the delivery of radiation therapy to cancer patients. Siam Review 41 (4), 721–744.

Trofimov, A., Unkelbach, J., DeLaney, T. F., Bortfeld, T., 2012. Visualization of a variety of possible dosimetric outcomes in radiation therapy using dose-volume histogram bands. Practical Radiation Oncology 2 (3), 164–171.

Unkelbach, J., Oelfke, U., 2004. Inclusion of organ movements in IMRT treatment planning via inverse planning based on probability distributions. Physics in Medicine and Biology 49 (17), 4005.

Wong, J. R., Grimm, L., Uematsu, M., Oren, R., Cheng, C. W., Merrick, S., Schiff, P., 2005. Image-guided radiotherapy for prostate cancer by ct–linear accelerator combination: Prostate movements and dosimetric considerations. International Journal of Radiation Oncology* Biology* Physics 61 (2), 561–569.

Yoon, M., Park, S. Y., Shin, D., Lee, S. B., Pyo, H. R., Kim, D. Y., Cho, K. H., 2007. A new homogeneity index based on statistical analysis of the dose–volume histogram. Journal of Applied Clinical Medical Physics 8 (2), 9–17.

Zaghian, M., Cao, W., Liu, W., Kardar, L., Randeniya, S., Mohan, R., Lim, G., 2017. Comparison of linear and nonlinear programming approaches for worst case dose and minmax robust optimization of intensity-modulated proton therapy dose distributions. Journal of Applied Clinical Medical Physics 18 (2), 15–25.

Zaghian, M., Lim, G., Liu, W., Mohan, R., 2014. An automatic approach for satisfying

dose-volume constraints in linear fluence map optimization for IMPT. Journal of Cancer Therapy 5 (2), 198.

Zaghian, M., Lim, G. J., Khabazian, A., 2018. A chance-constrained programming framework to handle uncertainties in radiation therapy treatment planning. European Journal of Operational Research 266 (2), 736–745.